Supporting Information for

Realization of Half-metallic Intrinsic Ferromagnetism with High Curie Temperatures by Low Oxidation State of Chromium in Cr_2TeX_2 (X = Br, I) Monolayers

Keke Mao[a, c], Shixiang Zu[a], Xiuling Li[b], Yehan Wang[a], Zhiming Li[a], Dawei Yan[a]**

[a]*School of Energy and Environment, Anhui University of Technology, Maanshan, Anhui 243032, China.*

[b]*School of Physics and Technology, Center for Quantum Transport and Thermal Energy Science, Institute of Physics Frontiers and Interdisciplinary Sciences, Nanjing Normal University, Nanjing 210023, China.*

[c]*Yida Intelligent Thermal Management Technology (Ma' anshan)Co.,Ltd, Maanshan, Anhui, China.*

Email: xlli@njnu.edu.cn, 305653720@qq.com

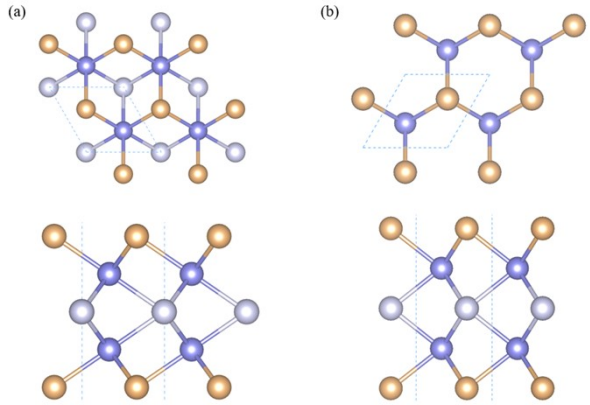

Fig. S1 Top and side views of M_2YX_2 monolayers configurations with (a) A_TA_T type and (b) A_HA_H type.

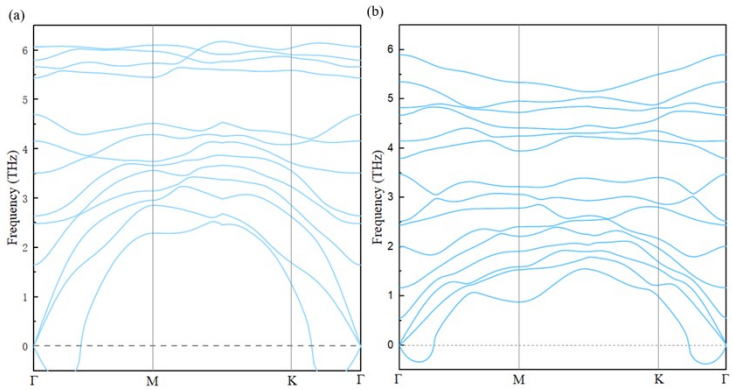

Fig. S2 Phonon dispersion for (a) A_TB_T Cr_2TeCl_2 and (b) A_TA_T Cr_2TeI_2 monolayers.

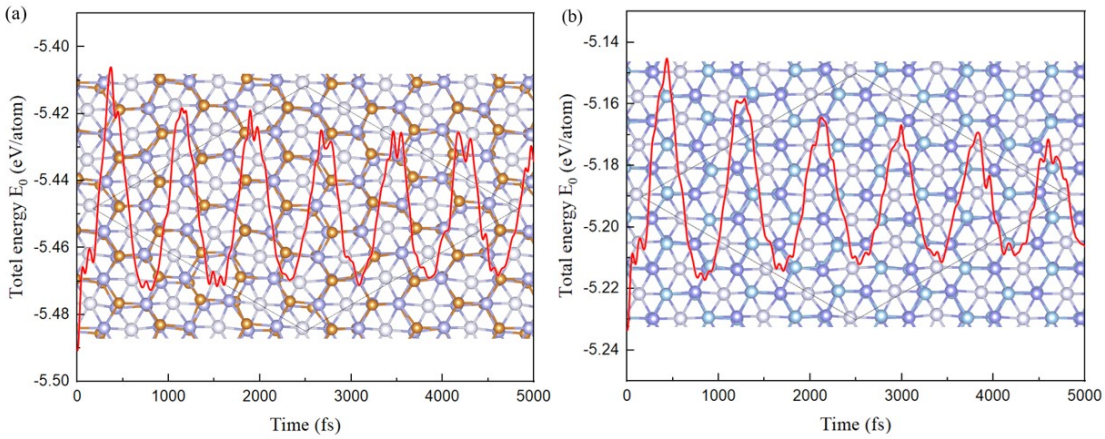

Fig. S3 AIMD simulations of a 5×5×1 supercell for (a) Cr_2TeBr_2 and (b) Cr_2TeI_2 monolayers at 300 K for 5 ps. Top views of the corresponding geometric structures after the AIMD simulation are shown, along with the energy fluctuations.

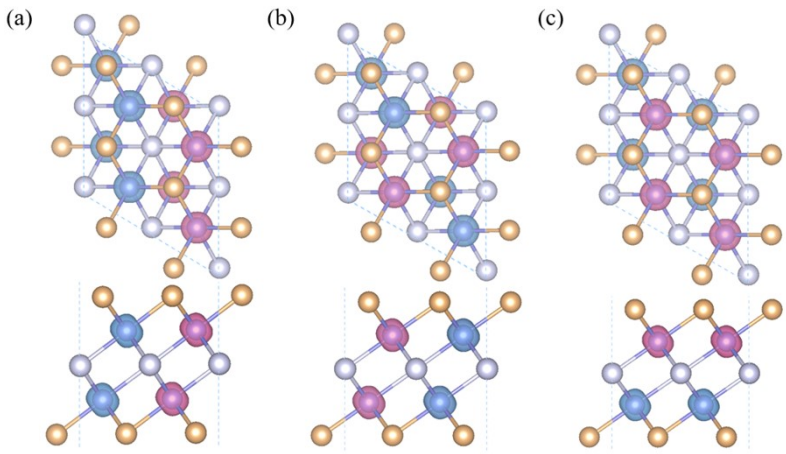

Fig. S4 Density of spin states for the antiferromagnetic states of Cr_2TeX_2 (X = Br, I, Se) monolayers, namely (a) AFM1, (b)AFM2, (c)AFM3. Red and blue represent spin-up and spin-down states, respectively.

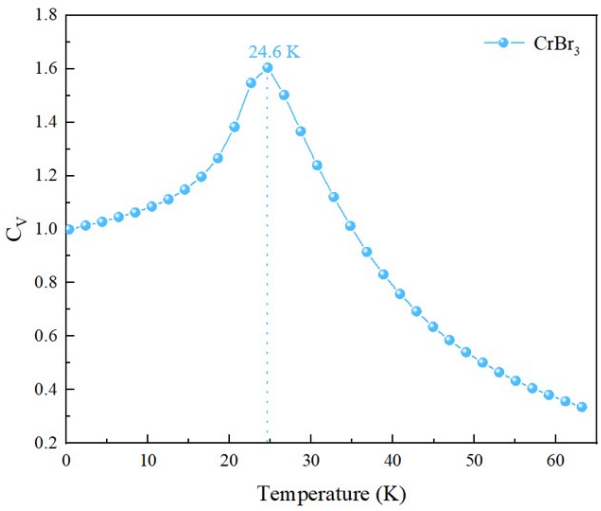

Fig. S5 Variation of specific heat capacity C_V with temperature for Cr_2Br_3 monolayer.

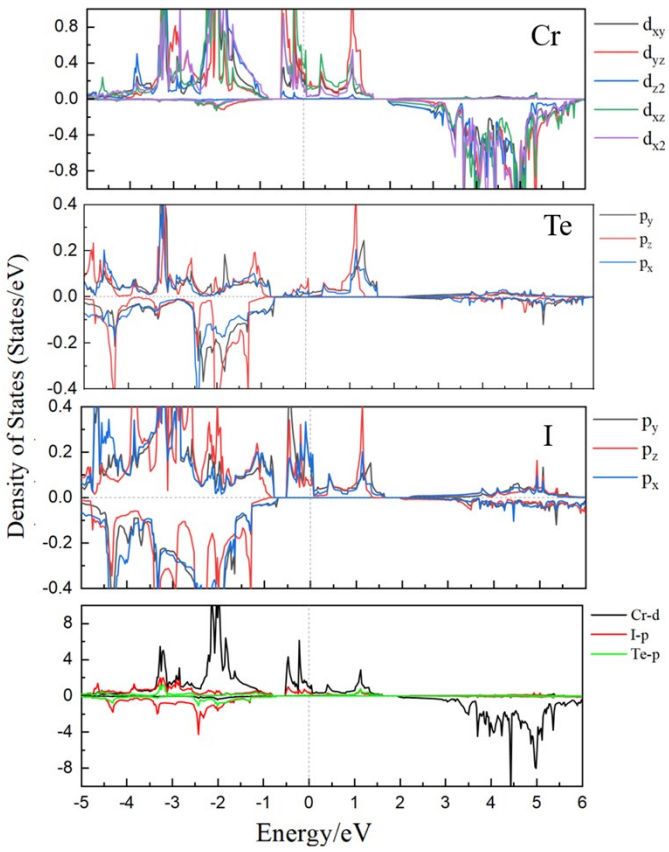

Fig. S6 Projected density of states for the Cr-d, Te-p, and I-p orbitals in the Cr_2TeI_2 monolayer.

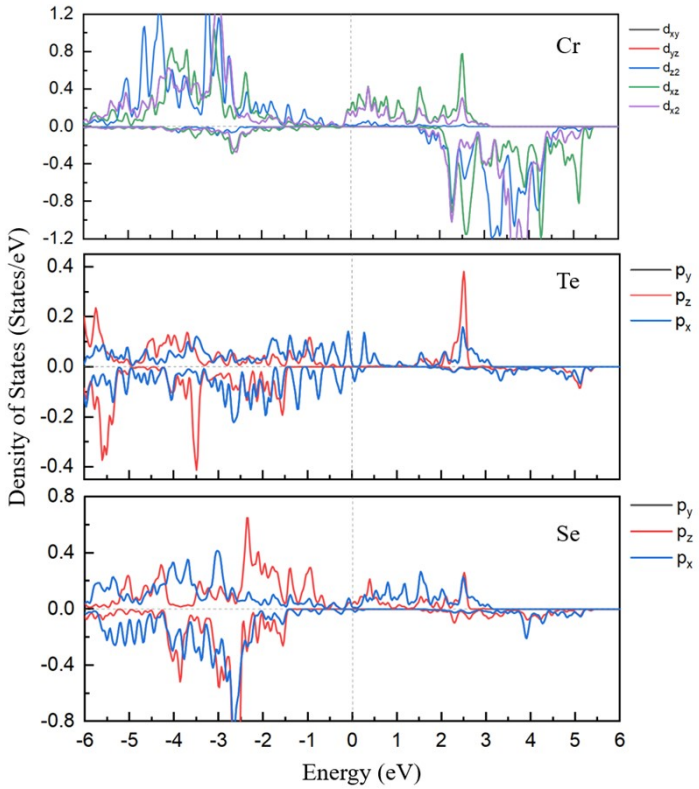

Fig. S7 Projected density of states for the Cr-d, Te-p, and I-p orbitals in the Cr_2TeSe_2 monolayer.

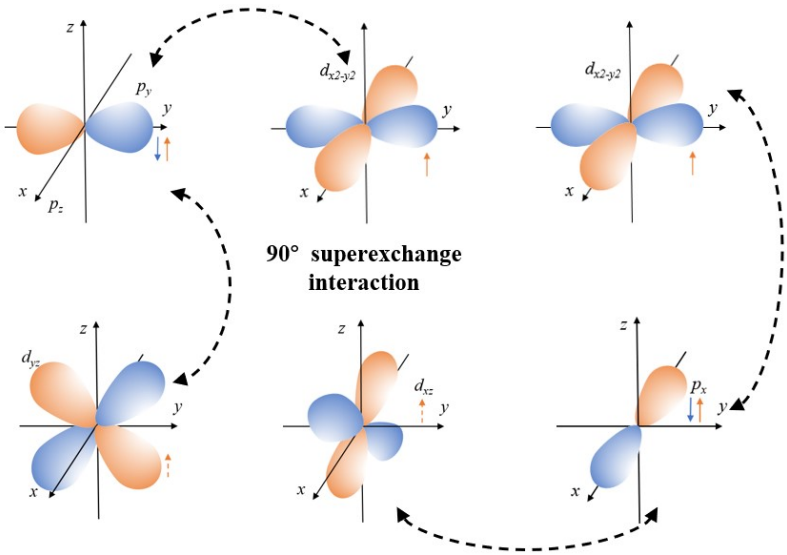

Fig. S8 Schematic of the potential 90° superexchange interaction of a Cr_2TeI_2 monolayer.

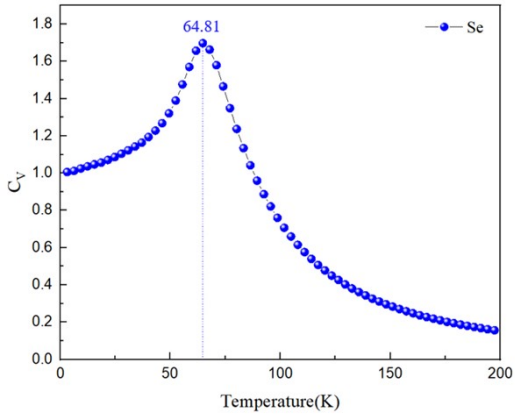

Fig. S9 Variation of specific heat capacity C_v with temperature for Cr_2TeSe_2 monolayer.

Section 1. Exchange coupling parameters methods and details

For the calculation of exchange coupling parameters, J_1, J_2 and J_3, the Heisenberg model are employed. [1, 2] These three exchange coupling parameters J_1, J_2 and J_3 are related to the total energy of the four magnetic states FM, AFM1, AFM2 and AFM3. The calculation relationship is as follows:

$$E_{FM} = (-24J_1 - 12J_2 - 12J_3)S^2 + E_0 \#(1)$$

$$E_{AFM1} = (8J_1 - 4J_2 + 12J_3)S^2 + E_0 \#(2)$$

$$E_{AFM2} = (8J_1 + 4J_2 - 12J_3)S^2 + E_0 \#(3)$$

$$E_{AFM3} = (-24J_1 + 12J_2 + 12J_3)S^2 + E_0 \#(4)$$

Meanwhile, the magnetic anisotropy parameter D_i can be calculated by

$$\frac{\{[E(001) - (100)] + E[(001) - (010)]\}}{2} = D_i S^2 \#(6)$$

The calculation results are shown in **Table S3**.

Section 2. Anomalous Hall conductivity calculation methods and details

The anomalous Hal conductivity was calculated for the material as follows:[3, 4]

$$\sigma_{xy} = \int_{BZ} \frac{d^d k}{(2\pi)^d} \Omega_z(k) \#(6)$$

where $\Omega_z(k)$ is the *z* component of the total Berry curvature of the occupied states at *k*,

$$\Omega_z(k) = -2Im \sum_{n \neq n'} f_{nk} \frac{\langle nk|v_x|n'k\rangle\langle n'k|v_y|nk\rangle}{(\omega_{n'} - \omega_n)^2} \#(7)$$

n' and n are the band indices, $\varepsilon_n = \hbar\omega_n$ is the band energy, v is the velocity operator, and f_{nk} is the equilibrium occupation function.

Section 3. Band center calculation methods and details

The *d* band center was calculated for the material as follows:

$$\varepsilon_d = \frac{\int_{-\infty}^{+\infty} E \cdot \rho_d(E) dE}{\int_{-\infty}^{+\infty} \rho_d(E) dE} \#(8)$$

where $\rho_d(E)$ is the density of states at different energies.

Section 4. 90° superexchange via Cr-Te/I-Cr in Cr_2TeI_2

For 90° *d-p-d* superexchange, since the Cr-d_{yz} and Cr-d_{xz} orbitals are degenerate and at the highest energy level, one of these orbitals is occupied while the other remains empty. If the d_{yz} orbital is empty, during the 90° superexchange process and in accordance with the molecular orbital symmetry matching principle (as shown in Fig. S8), one electron 'virtually' hops from the Te/I-p_y orbital to the empty Cr-d_{yz} orbital. Subsequently, another electron from the adjacent Cr ion's occupied d_{x2-y2} orbital 'virtually' hops to the Te/I-p_y orbital to fill up the "hole". Alternatively, if the d_{xz} orbital is empty, a similar 'virtual' hopping process takes place, with the key difference being the involvement of three distinct orbitals: Te/I-p_x, Cr-d_{xz}, Cr-$d_{x^2-y^2}$ orbitals. This is confirmed by the clear hybridization between the Cr-$d_{x^2-y^2/yz/xy}$ and Te/I-p_x/p_y orbitals, as shown in Fig. S6. Consider the first case: as the second electron from the Cr-$d_{x^2-y^2}$ orbital occupies the vacancy in the Te/I-p_y orbital created by the initial hopping

event, both electrons must align with the same spin orientation. Additionally, since Cr_2TeI_2 monolayer exhibits a FM ground state with a $3d^4$ half-filled orbital configuration, the four Cr-*d* orbitals maintain parallel spin alignment. Consequently, the hopping electrons must align their spins parallel to the *d*-orbitals of the adjacent Cr ions, leading to FM coupling between the neighboring Cr ions.

Table S1. The energy differences of 63 M_2YX_2 monolayers between the AFM and FM states (**ΔE_{AFM-FM}**/eV).

	Te-I	Te-Br	Te-Cl	Se-I	Se-Br	Se-Cl	S-I	S-Br	S-Cl
Ti	-0.703	-0.260	-0.183	-0.005	0	-0.009	0	0	0
V	-0.582	-0.326	-0.398	-0.750	-0.753	-0.770	-0.097	-1.421	-1.370
Cr	0.127	0.119	0.032	-0.315	-0.331	-0.317	-0.755	-0.748	-0.747
Mn	-0.698	-0.232	-0.231	-0.289	-0.289	-0.282	-0.132	-0.139	-0.271
Fe	-1.112	-1.232	-1.438	-0.557	-0.623	-1.477	-0.539	-0.536	-1.158
Co	0.117	-0.060	-0.631	-0.272	-0.066	-0.126	-0.321	-0.423	-0.650
Ni	0	-0.003	0.005	0	-0.015	0	0	0	-0.023

Table S2. The formation energy E_f (eV/atom) of FM M_2YX_2 monolayers with three different stacking structures.

Name	A_TB_T-type	A_TA_T-type	A_HA_H-type
Cr_2TeCl_2	-0.521	-0.502	-0.346
Cr_2TeBr_2	-0.411	-0.400	-0.204
Cr_2TeI_2	-0.242	-0.243	0.022
Co_2TeI_2	0.737	0.040	-0.340

Table S3. Spin polarized band center for five partial *d* orbitals of Cr in Cr_2TeI_2 monolayer.

Cr_2TeI_2 nanosheets Cr-d orbital centers (in eV)					
	d_{xy}	d_{yz}	d_{z2}	d_{xz}	d_{x2-y2}
Spin-up	-1.778	-1.450	-2.143	-1.466	-1.793
Spin-down	4.103	4.177	4.239	4.083	4.210
tot	0.758	1.096	0.504	1.052	0.888

Table S4. Spin polarized band center for five partial *d* orbitals of Cr in Cr_2TeSe_2 monolayer.

Cr_2TeSe_2 nanosheets Cr-d orbital centers (in eV)					
	d_{xy}	d_{yz}	d_{z2}	d_{xz}	d_{x2-y2}
Spin-up	-2.749	-2.056	-3.522	-2.056	-2.749
Spin-down	2.722	2.492	2.988	2.492	2.722

REFERENCES

1. *H. J. Xiang, S.-H. Wei and M. H. Whangbo, Physical Review Letters, 2008, 100.*
2. *H. Xiang, C. Lee, H.-J. Koo, X. Gong and M.-H. Whangbo, Dalton Trans., 2013, 42, 823-853.*
3. *S. Li, S.-S. Wang, B. Tai, W. Wu, B. Xiang, X.-L. Sheng and S. A. Yang, Physical Review B, 2021, 103.*
4. *Y. Yao, L. Kleinman, A. H. MacDonald, J. Sinova, T. Jungwirth, D.-s. Wang, E. Wang and Q. Niu, Physical Review Letters, 2004, 92.*